

Continuum Shell Model

Alexander Volya¹ and Vladimir Zelevinsky²

¹*Department of Physics, Florida State University, Tallahassee, FL 32306-4350, USA*

²*NSCL and Department of Physics and Astronomy,
Michigan State University, East Lansing, MI 48824-1321, USA*

(Dated: August 27, 2018)

The Continuum Shell Model is an old but recently revived method that traverses the boundary between nuclear many-body structure and nuclear reactions. The method is based on the non-Hermitian energy-dependent effective Hamiltonian. The formalism, interpretation of solutions and practical implementation of calculations are discussed in detail. The results of the traditional shell model are fully reproduced for bound states; resonance parameters and cross section calculations are presented for decaying states. Particular attention is given to one- and two-nucleon reaction channels including sequential and direct two-body decay modes. New calculations of reaction cross sections and comparisons with experimental data for helium and oxygen isotope chains are presented.

PACS numbers: 21.60.Cs, 24.10.Cn, 24.10.-i

Keywords: Continuum Shell Model, reactions

I. INTRODUCTION

New horizons are in sight in the field of nuclear physics as we move away from the line of nuclear stability. In the everyday experience we observe only a tiny fraction of the nuclear world, while the recent advances in observational techniques reveal a hidden realm of extraordinary nuclear complexes. The term “exotic” is commonly used to highlight the unusual nature of newly discovered nuclear systems where structure and stability are governed by intricate interplay of quantum many-body structure and dynamics of nuclear reactions. Weakly bound nuclei and unstable resonances appear as important links in the chain of nuclear evolution in cosmos, their structure and properties are central for energy generation in stars and production of elements in the universe. Furthermore, the quantum objects of mesoscopic nature are common to many fields of science including but not limited to atoms and molecules, nanoscale condensed matter systems, atomic clusters, atoms in traps, and prototypes of quantum computers [1]. In many applications to mesoscopic systems one needs to understand and utilize the features of marginal stability and strong coupling between discrete structure and continuum.

Mean field along with corresponding shell structure is a starting point in the theoretical analysis of a quantum many-body system. The shell structure itself becomes exotic on the borderline of the continuum [2, 3, 4, 5]. Single-particle, pairwise and cluster excursions into the continuum become essential forming halo states and resulting in complex mixing of internal many-body states and continuum configurations. The problems of continuum shell model (CSM), or combining the description of reactions with the structure calculations, have been discussed almost since the dawn of the shell model, and summarized in the classical text [6]. However, only recently, fuelled by the discoveries of exotic systems, acute need in theoretical understanding, and growing computational capabilities, this subject received due attention, so that significant advances have been made during last years. In this work we concentrate on the version of the CSM [7, 8] that is going back to the Feshbach projection formalism [9, 10, 11, 12] and, even much earlier, to the approach by Weisskopf and Wigner [13] and works in atomic physics by Rice [14] and Fano [15, 16]. Alternative formulations, such as [17, 18, 19, 20], see a review [21], were also successfully developed recently.

The specific attractive features of the approach discussed below are the natural unification of structure and reactions, full agreement with the results of the traditional shell model (SM) in the discrete spectrum, correct energy behavior of resonance widths and reaction cross sections near thresholds, self-consistent consideration of isotope chains, and exact unitarity of the scattering matrix. At this point we use the standard residual interactions adjusted in numerous applications of the conventional SM, although the problem of better interactions in the continuum remains open (the first steps in this direction were made in Ref. [22]).

We organize the discussion here starting with the formal description of the CSM approach in the following section; this will be the formalism that we imply under the term CSM throughout this work. In Sec. II we also discuss mathematical details of the formulation, relation to observables and the unitarity of the scattering matrix. Sec. III is devoted to the detailed consideration of different parts of the interaction; we consider the limit of the conventional shell model one-body decay channels, and sequential and direct two-body channels. The realistic applications are shown and compared with experiment in Sec. IV.

II. FORMULATION OF THE CONTINUUM SHELL MODEL

A. Effective Hamiltonian

In what follows we assume that the many-body Hilbert space is spanned by Slater determinants constructed from the single-particle (s.p.) orbitals $|j\rangle$ in the mean field. Using the notations of secondary quantization we denote the s.p. creation and annihilation operators for discrete orbitals as b_j^\dagger and b_j labelled by a combined discrete label j . For the continuum states we use s.p. operators $b_j^\dagger(\epsilon)$ and $b_j(\epsilon)$ which are labelled with the discrete index j and the continuous s.p. energy variable ϵ . If properly constructed for a mean-field potential, see below the discussion related to one-body reactions, these states are automatically orthogonal and form a complete set. In this work, however, we require only separate orthogonality of the bound states, $[b_j, b_{j'}^\dagger]_+ = \delta_{jj'}$, and of the continuum states normalized according to $[b_j(\epsilon), b_{j'}^\dagger(\epsilon')]_+ = \delta(\epsilon - \epsilon') \delta_{jj'}$.

The full many-body space can be separated into two parts. The set of N -particle bound states $|1; N\rangle = b_{j_1}^\dagger \dots b_{j_N}^\dagger |0\rangle$ forms the ‘‘internal’’ space, \mathcal{P} , where the index $1 = \{j_1, j_2 \dots j_N\}$ labels the Slater determinant, the m -scheme representation in the SM terminology. The remaining space, \mathcal{Q} , is the ‘‘external’’ continuum, i.e. many-body states which contain one or more continuum s.p. orbitals. The external many-body states $|c, E\rangle$ are labelled by total continuum energy E and the set of asymptotic variables c that defines a reaction channel (it includes the characteristics of the residual nucleus). The channel variable c is discrete only in the case of the one-body decay where energy conservation fully determines energies of the two decay products. In general this variable is continuous, containing relative energies or momenta of decay products needed for full specification of the final state. In the description of the formalism below we use notations \sum_c and $\delta_{cc'}$ which in the case of the continuous channel variables should be interpreted as $\int dc$ and $\delta(c - c')$, respectively. In Sec. III D, where channel c in the two-body decay implies the presence of the relative energy variable, the sum over channels is explicitly given in terms of an integral. By construction, the many-body states in \mathcal{P} - and \mathcal{Q} - spaces are mutually orthogonal and normalized as

$$\langle 1|2\rangle = \delta_{12}, \quad \langle c; E|c'; E'\rangle = \delta_{cc'} \delta(E - E'). \quad (1)$$

Within the total space $\mathcal{P} + \mathcal{Q}$, we solve the stationary Schrödinger equation

$$H|\alpha; E\rangle = E|\alpha; E\rangle, \quad (2)$$

where the full wave function $|\alpha; E\rangle$ is in general a superposition of internal states $|1\rangle$ and external states $|c; E'\rangle$,

$$|\alpha; E\rangle = \sum_1 \alpha_1(E) |1\rangle + \sum_c \int dE' \alpha_c(E'; E) |c; E'\rangle. \quad (3)$$

The Hamiltonian H has parts acting within and across \mathcal{P} and \mathcal{Q} spaces, $H = H_{\mathcal{P}\mathcal{P}} + H_{\mathcal{P}\mathcal{Q}} + H_{\mathcal{Q}\mathcal{Q}}$. The external states can be eliminated by introducing a propagator that acts exclusively within \mathcal{Q} space,

$$G_{\mathcal{Q}\mathcal{Q}}(E) = \frac{1}{E - H_{\mathcal{Q}\mathcal{Q}} + i0}, \quad (4)$$

where the infinitesimal imaginary displacement selects the appropriate boundary conditions for the scattering problem. Next we assume that the channel labels c correspond to the eigenchannels [23] in the \mathcal{Q} space, $H_{\mathcal{Q}\mathcal{Q}}|c; E\rangle = E|c; E\rangle$. Then the Schrödinger equation (2) ‘‘projected’’ into the subspace \mathcal{P} becomes

$$\sum_2 \left[\langle 1|H|2\rangle + \sum_c \int dE' \frac{\langle 1|H - E|c; E'\rangle \langle c; E'|H - E|2\rangle}{E - E' + i0} - \delta_{12} E \right] \alpha_2 = 0. \quad (5)$$

The amplitude of the continuum admixture in the full wave function (3) is

$$\alpha_c(E'; E) = \frac{\sum_1 \alpha_1(E) A_1^c(E', E)}{E - E' + i0}, \quad (6)$$

where we introduced notations for the $H_{\mathcal{P}\mathcal{Q}}$ coupling amplitude

$$A_1^c(E', E) = \langle 1|H - E|c; E'\rangle. \quad (7)$$

This amplitude depends on the continuum variable of energy E' and running energy E . As follows from the definition (7), there is no explicit E -dependence when internal and external spaces are orthogonal. However, the important

E' -dependence remains; the kinematic factors included in the definition of the channel states $|c; E'\rangle$ ensure that the phase space shrinks to zero and the channel c becomes closed below threshold energy E_c characteristic for a given channel. Whence, the amplitudes A_1^c vanish at $E' < E_c$.

The set of equations (5) for coefficients α_1 looks as an eigenvalue problem with the effective Hamiltonian matrix \mathcal{H} in the intrinsic space defined as

$$\langle 1|\mathcal{H}(E)|2\rangle = \langle 1|H|2\rangle + \sum_c \int dE' \frac{A_1^c(E', E) A_2^{c*}(E', E)}{E - E' + i0}. \quad (8)$$

The integral in Eq. (8) can be further decomposed into its Hermitian part (principal value), $\Delta(E)$, and the anti-Hermitian part, $-(i/2)W(E)$,

$$\sum_c \int dE' \frac{A_1^c(E', E) A_2^{c*}(E', E)}{E - E' + i0} = \sum_c \text{P.v.} \int dE' \frac{A_1^c(E', E) A_2^{c*}(E', E)}{E - E'} - i\pi \sum_{c(\text{open})} A_1^c(E) A_2^{c*}(E), \quad (9)$$

where $A_1^c(E) \equiv A_1^c(E, E)$. Thus, the effective Hamiltonian for the \mathcal{P} space (10) takes form

$$\mathcal{H}(E) = H_{\mathcal{P}\mathcal{P}} + \Delta(E) - \frac{i}{2} W(E), \quad (10)$$

The resulting dynamics generated by the effective Hamiltonian (10) contains a usual \mathcal{P} -space contribution that we identify here with the traditional SM corrected by the virtual “off-shell” excitations into the continuum via the self-energy term,

$$\langle 1|\Delta(E)|2\rangle = \sum_c \text{P.v.} \int dE' \frac{A_1^c(E', E) A_2^{c*}(E', E)}{E - E'}, \quad (11)$$

and supplemented by the anti-Hermitian term,

$$\langle 1|W(E)|2\rangle = 2\pi \sum_{c(\text{open})} A_1^c(E) A_2^{c*}(E), \quad (12)$$

that represents the irreversible departure into \mathcal{Q} -space, i.e. decays; see Fig. 1. The term W that comes from the poles in integration (8), has a factorized form, which is shown below to relate to conservation of probability and unitarity of the scattering matrix. The amplitudes $A^c(E)$ here represent on-shell processes that depend only on one energy parameter and correspond to real decays with energy conservation, $E' = E$. These poles in integration appear only when running energy E is above the decay threshold E_c for a channel c . The channels where decays are allowed are referred to as open. At $E \rightarrow E_c + 0$ the amplitudes A_1^c vanish due to the kinematic factors implicitly included into their definition.

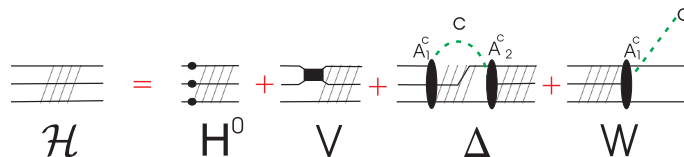


FIG. 1: (Color online) Diagrammatic equation for the full Hamiltonian corresponding to the dynamics in the \mathcal{P} space, Eq. (10). Parts H^0 and V on the figure indicate the one- (s.p. energies) and two-body parts of the internal Hamiltonian $H_{\mathcal{P}\mathcal{P}}$.

B. Scattering matrix and unitarity

The “outside” view from the reaction side of the problem is equally important. In accordance with general scattering theory, the transition matrix,

$$T^{cc'}(E) = \sum_{12} A_1^{c*}(E) \left(\frac{1}{E - \mathcal{H}(E)} \right)_{12} A_2^c(E), \quad (13)$$

describes the process that starts in the entrance channel c' with amplitude $A_2^{c'}$ originated from the interaction $H_{\mathcal{P}\mathcal{Q}}$, continues through internal propagation within the \mathcal{P} -space driven by the non-Hermitian energy-dependent effective

Hamiltonian (10) (with all excursions into \mathcal{Q} space included), and ends by exit to the channel c described by the amplitude $A_1^{c*}(E)$. The scattering matrix can be written as

$$S^{cc'}(E) = \exp(i\xi_c) \left\{ \delta^{cc'} - 2\pi i T^{cc'}(E) \right\} \exp(i\xi_{c'}). \quad (14)$$

The additional phase shifts $\xi_c(E)$ describe the potential scattering or a contribution of remote resonances outside of the valence space of the model.

The factorized nature of the non-Hermitian contribution to the effective Hamiltonian is the key for conserving the unitarity of the S matrix [24]. This can be demonstrated by considering the propagator for the effective Hamiltonian

$$\mathcal{G}(E) = \frac{1}{E - \mathcal{H}} \quad (15)$$

generated from the unperturbed propagator for the full Hermitian part,

$$G(E) = \frac{1}{E - H_{\mathcal{P}\mathcal{P}} - \Delta(E)}. \quad (16)$$

With $W = 2\pi\mathbf{A}\mathbf{A}^\dagger$, where \mathbf{A} represents a channel matrix (a set of columns of vectors A_1^c for each channel c), we iterate the Dyson equation

$$\mathcal{G} = G - (i/2)GW\mathcal{G} \quad (17)$$

and, due to the factorized form of W , come to

$$\mathcal{G} = G - i\pi G\mathbf{A} \frac{1}{1 + i\pi\mathbf{A}^\dagger G\mathbf{A}} \mathbf{A}^\dagger G, \quad (18)$$

that is called the Woodbury equation in mathematical literature.

The transition matrix, $T = \mathbf{A}^\dagger \mathcal{G} \mathbf{A}$, can then be written with the aid of the matrix $R = \mathbf{A}^\dagger G \mathbf{A}$ that is analogous to the R -matrix of standard reaction theory. The unitarity of S -matrix follows directly from these equations, see also [25],

$$T = \frac{R}{1 + i\pi R}, \quad S = \frac{1 - i\pi R}{1 + i\pi R}. \quad (19)$$

C. Energy dependence and resonances

The effective Hamiltonian of Eq. (10) is energy-dependent: at each scattering energy E its running eigenvalues are complex numbers $\mathcal{E}_\alpha(E)$. This highlights the structure in Eq. (3) that the eigenstate is a superposition of internal states and asymptotic decay states that have right energy. The relatively small, and numerically tractable, dimension of basis states, in exchange for non-Hermiticity and energy dependence, is a noteworthy advantage of this method as compared to direct discretization of continuum used in other approaches.

The eigenvalue problem involving a complex matrix of a general form requires finding two sets of adjoint eigenvectors: left, $|\alpha\rangle$, and right, $|\tilde{\alpha}\rangle$. They satisfy

$$\mathcal{H}|\alpha\rangle = \mathcal{E}_\alpha|\alpha\rangle \quad \text{and} \quad \langle\tilde{\alpha}|\mathcal{H} = \mathcal{E}_\alpha^*\langle\tilde{\alpha}|. \quad (20)$$

The left and right eigenstates correspond to time reversed motions; they no longer have to coincide because the \mathcal{T} -invariance in the internal space is broken by irreversible decays. The global symmetry with respect to the direction of time is however maintained by the full Hamiltonian that includes the products of reactions. As a result, the left and right eigenstates have the wave functions interrelated by complex conjugation which is the time inversion operation. The Hermitian conjugation of the Hamiltonian switches the roles of left and right; the same effect can be reproduced by selecting an advanced propagator boundary condition in (4) discussed earlier. The biorthogonality relation is given by $\langle\tilde{\alpha}|\beta\rangle = \delta_{\alpha\beta}$; similarly, the expectation value of an operator X is $\langle\tilde{\alpha}|X|\beta\rangle$. These properties, the formalism of CSM and its interpretation become transparent in the one-body problem discussed below in Sec. III A; for further notes on this topic we refer to [26].

There are various interpretations of eigenvalues $\mathcal{E}_\alpha(E)$ of Eq. (5). Only for bound states below all decay thresholds a condition $\mathcal{E}_\alpha(E) = E$ is satisfied since $W = 0$. With non-zero W , the eigenvalues of the effective Hamiltonian are in general complex,

$$\mathcal{E}_\alpha(E) = E_\alpha(E) - \frac{i}{2} \Gamma_\alpha(E), \quad (21)$$

describing the quasistationary states. These resonances and their widths $\Gamma_\alpha \geq 0$ satisfy the Bell-Steinberger relation

$$\langle \tilde{\alpha} | W | \alpha \rangle = \Gamma_\alpha, \quad (22)$$

where the left hand side can be expressed through the amplitudes A_1^\dagger transformed to the biorthogonal basis of quasistationary states $|\alpha\rangle$.

The continuation of the original problem to the lower part of the complex energy plane, $E \rightarrow \mathcal{E} = E - (i/2)\Gamma$ allows the condition

$$\mathcal{E}_\alpha(\mathcal{E}) = \mathcal{E}. \quad (23)$$

The complex energy roots here can be identified with the poles in the scattering matrix (14), and the states correspond to many-body resonant Siegert states [27] since by construction the eigenstate (3) is a regular function with outgoing asymptotics. One can also use the Breit-Wigner approach [28] and identify resonances differently, with a condition

$$\text{Re}[\mathcal{E}_\alpha(E)] = E, \quad \Gamma_\alpha = -2\text{Im}[\mathcal{E}(E)]. \quad (24)$$

In the limit of small imaginary part (narrow resonances), both definitions are equivalent. However in general the difficulty in parameterizing the resonance width and centroid energy is related to the non-exponential character of decay caused by the energy dependence of the Hamiltonian parameters. Wide resonances cover broad regions of energy and therefore are particularly affected by this dependence. This leads to the non-generic and asymmetric shape of the resonance cross section that makes standard Breit-Wigner or Gaussian parameterizations inappropriate.

With either definition, Eqs. (23) or (24) for resonant states are complicated sets of nonlinear equations. In some cases [7] the condition (23) may lead to unphysical solutions. For the realistic calculations shown in Sec. IV we select the Breit-Wigner definition (24) and implement an iterative approach starting from the energy determined by the conventional SM with $W = 0$. Although it is convenient to express the solutions in terms of resonant states, the parameters are definition-dependent and become misleading for broad states or in the case of overlapping resonances when interference is important. In these cases one should turn to the observable scattering cross section determined by the S -matrix of Eq. (14). The computation of the scattering cross section is a problem of matrix inversion which is linear in accordance with physical principles, but it has to be done at each energy which can make this task numerically unstable for narrow resonances. The cross sections can be calculated using the R -matrix of Eq. (19) and the Woodbury equation in which case complex arithmetics can be avoided. We will see complementary pictures that can be obtained by calculating the cross section and via resonance parameters coming from the diagonalization of the effective Hamiltonian in the example shown in Sec. IV.

III. FROM HAMILTONIAN TO DYNAMICS

The derivation above is based on the decomposition of the full Hamiltonian into $H = H_{\mathcal{P}\mathcal{P}} + H_{\mathcal{P}\mathcal{Q}} + H_{\mathcal{Q}\mathcal{Q}}$. Another useful classification traditional to the SM is by the types of many-body processes it can generate. At this stage we restrict the interactions by one- and two-body and limit the space \mathcal{Q} by the states with only one or two nucleons in continuum. The typical shell model limitations by few valence shells are imposed on the intrinsic space \mathcal{P} . In this framework we define the full Hamiltonian and discuss processes associated with each of the terms.

Our discussion here, however, does not touch the lack of knowledge of the effective interaction. Although sophisticated methods of deriving the effective interactions were suggested [22, 29], the best results and the most predictive power in the conventional SM come from the phenomenological interactions, such as USD [30], fitted to experimental data. The situation becomes increasingly more complicated when effective interactions involving continuum are to be used [26]. In this work we identify the internal interaction $H_{\mathcal{P}\mathcal{P}}$, together with the Hermitian self-energy term Δ included, with a shell model Hamiltonian of the form

$$H_{\mathcal{P}\mathcal{P}} + \Delta = \sum_j \epsilon_j b_j^\dagger b_j + \frac{1}{4} \sum V(j_1 j_2; j_3 j_4) b_{j_1}^\dagger b_{j_2}^\dagger b_{j_3} b_{j_4}. \quad (25)$$

The parameters, s.p. energy levels and antisymmetrized two-body matrix elements, are known from fits to experimental data, such as [30], see also review [2], and available from interaction libraries, such as [31]. The energy dependence of these parameters that comes from $\Delta(E)$ is ignored here since it has not been included in the fitting process. As demonstrated below this dependence is weak and smooth function of energy. Defining the internal Hamiltonian in this way we guarantee that below thresholds the CSM provides the results identical to the well established SM with effective interactions. Above thresholds, the shell model interactions were fitted to experimental data using R -matrix

analysis that identifies interactions (25) in the same way, Eq. (19). The consistent readjustment of shell model interaction parameters taking into account energy dependence of Hermitian part is beyond the scope of this paper but remains a subject of future work.

In this work we assume that the Hamiltonian describing the motion of nucleons in the continuum is purely single-particle

$$H_{\mathcal{Q}\mathcal{Q}} = \sum_j \int d\epsilon \epsilon b_j^\dagger(\epsilon) b_j(\epsilon). \quad (26)$$

The asymptotic one- and two-particle continuum states considered in this work are antisymmetrized products of internal eigenstates α of the residual nucleus and the wave function(s) of particle(s) in the continuum. The states in one-body channels,

$$|c; E\rangle = b_j^\dagger(\epsilon_j) |\alpha; N-1\rangle, \quad E = E_\alpha + \epsilon_j, \quad (27)$$

are labelled by energy E and the discrete channel index c that combines the s.p. quantum numbers j and characteristics α for the eigenstate of an $(N-1)$ -particle daughter system.

The assumption (26) allows one to express similarly the two-nucleon channel states,

$$|c; E\rangle = b_j^\dagger(\epsilon) b_{j'}^\dagger(\epsilon') |\alpha; N-2\rangle, \quad (28)$$

characterized by the total energy $E = E_\alpha + \epsilon_j + \epsilon_{j'}$ combined of the daughter binding energy E_α and energies of emitted nucleons in s.p. states j and j' . Here the channel c contains in addition information on continuous relative energy distribution between emitted particles. Within this work we do not consider cases when both particles in the continuum are charged thus the assumptions in Eqs. (26) and (28) are sufficient. The generalization for bound states of two particles in the continuum is relegated to the next stage.

A. Single-particle decay and resonances

Now we need to define the interaction $H_{\mathcal{P}\mathcal{Q}}$ responsible for coupling of intrinsic space with the continuum. We start with the one-body part and associate it with some potential V assuming this potential to be spherically symmetric.

We first treat a pure s.p. problem of a particle moving in the mean field or independent particle shell model. The generalization covering all s.p. channels in many-body cases is straightforward and discussed in what follows. Of course, this subject is extensively covered by textbooks [32, 33, 34]. The purpose of the formulation presented here is to emphasize the conceptual identity between the full CSM and its trivialized version represented by a single particle in a potential. The notions and definitions of resonances, scattering matrix and its poles, time reversal and non-Hermiticity already appear in this simplest case. This section also highlights some technical details used later for the s.p. part in the full CSM including the generic threshold behavior of the decay amplitudes.

In the coordinate representation the Schrödinger equation for the radial part of the s.p. wave function,

$$\langle \mathbf{r} | b_j^\dagger | 0 \rangle = [Y_l \chi]_j \frac{u_j(r)}{r}, \quad (29)$$

where Y_l and χ represent the angular and spin parts coupled to total angular momentum j , is

$$\left\{ -\frac{d^2}{dr^2} + \frac{l(l+1)}{r^2} + 2\mu \left[V(r) + e^2 \frac{Zz}{r} \right] \right\} u_j(r) = k^2 u_j(r), \quad (30)$$

where $k^2 = 2\mu\epsilon$, μ is the reduced mass, z and Z are charges of the particle and of the residual nucleus, respectively. The spin-orbit part can be included here assuming that the potential $V(r)$ depends on l and the spin orientation which in our notations are hidden in the s.p. index j .

For Eq. (30) with $V(r) = 0$, we have the regular, $F_l(kr)$, $F_l(0) = 0$, and the irregular, $G_l(kr)$, solutions as Coulomb wave functions with the charge parameter $\eta = \mu\alpha Zz/k$. For a neutral particle, $z = 0$, the regular and irregular solutions can be expressed in terms of spherical Bessel and Neumann functions,

$$F_l(kr) = kr j_l(kr), \quad G_l(kr) = -kr n_l(kr). \quad (31)$$

The two independent solutions are related by the Wronskian,

$$G_l \frac{d}{d(kr)} F_l - F_l \frac{d}{d(kr)} G_l = 1. \quad (32)$$

Thus, the \mathcal{Q} space states are energy-normalized regular solutions,

$$\langle \mathbf{r} | j; \epsilon \rangle = \langle \mathbf{r} | b_j^\dagger(\epsilon) | 0 \rangle = [Y_l \chi]_j \sqrt{\frac{2\mu}{\pi k}} \frac{F_l(kr)}{r}. \quad (33)$$

Following the definition in Eq. (7), the s.p. decay amplitude is

$$a_j(\epsilon_j, \epsilon) = \langle j | H_{\mathcal{P}\mathcal{Q}} - \epsilon | j; \epsilon_j \rangle = \sqrt{\frac{2\mu}{\pi k_j}} \int_0^\infty dr F_l(k_j r) [V(r) + \epsilon_j - \epsilon] u_j(r). \quad (34)$$

A positive energy internal state $u_j(r)$ decays with the width $\gamma_j = 2\pi a_j^2$ determined by the above equation; under this choice of phases, the decay amplitudes are real. The s.p. amplitude has only one index j .

This result for the decay width can be reproduced through the equivalent consideration of the on-shell scattering process. Let us introduce incoming and outgoing (Coulomb) waves $O_l^\pm(r) = G_l(r) \pm iF_l(r)$. Consider a resonant state u_j ; since through the rest of this subsection we concentrate on a state with a given set of s.p. quantum numbers j we will omit this subscript in notations, the orbital momentum subscript l which is a part of the combined index j is also omitted. The state u can be normalized as a discrete state when the decaying component that obeys the Siegert [27] outgoing wave boundary condition,

$$\lim_{r \rightarrow \infty} u(r) = \mathcal{N} O^+(kr), \quad (35)$$

is neglected. Then the outgoing flux normalized by velocity determines the decay width

$$\gamma = 2\pi a^2 = \frac{k}{\mu} |\mathcal{N}|^2. \quad (36)$$

It follows from here that the asymptotics of the decaying states are given by the decay amplitude,

$$\lim_{r \rightarrow \infty} u(r) = -\sqrt{\frac{2\pi\mu}{k}} a(\epsilon) O^+(kr), \quad (37)$$

where we selected a phase to be consistent with the previous definition. Using the Wronskian relations, the outgoing part can be extracted from the wave function u_j leading to

$$a(\epsilon) = -\sqrt{\frac{1}{2\pi\mu k}} \left(u \frac{dF}{dr} - F \frac{du}{dr} \right) \Big|_{r \rightarrow \infty}. \quad (38)$$

This equation is identical to Eq. (34) since the Schrödinger equation (30) that must be used to determine the outgoing component guarantees that

$$\frac{d}{dr} \left(u \frac{dF}{dr} - F \frac{du}{dr} \right) = -2\mu FV(r)u(r), \quad (39)$$

where F is any of the Coulomb wave functions.

The eigenstate wave function in the asymptotics can be expressed via the s.p. scattering phase shift, $u_j(\epsilon) \sim \cos(\delta_j)F_l + \sin(\delta_j)G_l$. The related S -matrix then can be found as

$$S = \exp(2i\delta) = \frac{u \frac{d}{dr} O^- - O^- \frac{d}{dr} u}{u \frac{d}{dr} O^+ - O^+ \frac{d}{dr} u} \Big|_{r \rightarrow \infty} \quad (40)$$

that is consistent with definitions (13) and (14). The poles of the scattering matrix correspond to the condition of the regular wave function with the outgoing wave in asymptotics. Just as in the general case in Sec. II, this can not be satisfied at real energy, while if the problem is taken into a complex energy plane, $k \rightarrow \kappa = k - i\kappa$ and $\epsilon \rightarrow e = \epsilon - i\gamma/2$, the discrete set of solutions emerges. Thus, the resonance energy ϵ and the width γ can be defined as real and imaginary parts, respectively, of the complex energy which is the pole of the scattering matrix. Consistent with the general theory, the time reversed problem is physically equivalent; the boundary condition then is that the wave function be regular at the origin and represent an incoming wave in asymptotics. This is a \mathcal{T} -reversed state, with the corresponding “left” momentum eigenvalue $\tilde{\kappa}$ that is related to that of the “right” eigenstate as $\tilde{\kappa} = -\kappa^*$. This agrees with the symmetry properties of the S matrix,

$$S(\kappa) = S^*(-\kappa^*) = S^{-1}(-\kappa), \quad (41)$$

and assures that left and right energy eigenvalues are complex conjugate.

Numerically, the decay amplitudes can be calculated directly from (34) or (38); it has been demonstrated in [35] for proton emitters that these methods are equally effective in practice. The effective non-Hermitian s.p. Hamiltonian can be solved resulting in Gamow states via an iterative procedure based on the Green's function, similar to the approach discussed in [36, 37]. Green's function is constructed for the free particle case $V = 0$ using Coulomb functions at some momentum k_0 and the Siegert boundary conditions,

$$\mathcal{G}(r, r') = \frac{1}{k_0} F(k_0 r_{<}) O^+(k_0 r_{>}). \quad (42)$$

The $r_{<}$ and $r_{>}$ denote the smaller and the larger of r and r' , respectively. The integral equation for the resonant state becomes

$$u(r) = \int_0^\infty \mathcal{G}(r, r') [\kappa^2 - k_0^2 - 2\mu V(r')] u(r') dr'. \quad (43)$$

This leads to the following equation for the radial part $u(r)$:

$$u(r) = \frac{1}{k_0} F(r) \left\{ \int_r^\infty O^+(r') [\kappa^2 - k_0^2 - 2\mu V] u(r') dr' \right\} + \frac{1}{k_0} O^+(r) \left\{ \int_0^r F(r') [\kappa^2 - k_0^2 - 2\mu V] u(r') dr' \right\}. \quad (44)$$

The complex momentum κ is determined self-consistently with the decay flux defined by the outgoing component in the above equation.

B. Threshold behavior

The behavior of the decay width and the self-energy term $\Delta(\epsilon)$ in the vicinity of threshold is particularly important. The one-body decay is an instructive example of the CSM at work. Following the above definitions we evaluate

$$\int_0^\infty d\epsilon_j \frac{|a_j(\epsilon_j, \epsilon)|^2}{\epsilon - \epsilon_j + i0} = \Delta(\epsilon) - \frac{i}{2} \gamma(\epsilon) \quad (45)$$

in the vicinity of the single-particle threshold at zero energy using Eq. (34) which we decompose as

$$a_j(\epsilon_j, \epsilon) = \langle j|V|j; \epsilon_j \rangle + (\epsilon_j - \epsilon) \langle j|j; \epsilon_j \rangle. \quad (46)$$

Only the first term in (46) leads to a pole in Eq. (45). The main contribution comes from low-energy scattering states, namely in the limit when the de Broglie wavelength of the scattered particle exceeds the range of the potential. For a charged particle, the energy behavior of the amplitude (34) follows from that of the regular Coulomb function. For a neutral particle, in this limit $F_l = (kr)^{l+1}/(2l+1)!! \propto \epsilon^{(l+1)/2}$. Thus, we can assume that

$$\langle j|V|j; \epsilon_j \rangle = \varkappa_j (\sqrt{\epsilon_j})^{l+1/2}, \quad (47)$$

where the constant \varkappa_j is

$$\varkappa_j = \frac{(2\mu)^{(l+3/2)/2}}{\sqrt{\pi}(2l+1)!!} \int_0^\infty r^{l+1} V(r) u_j(r) dr. \quad (48)$$

In the integral (45) only the term $\propto \varkappa^2$ contains the contribution from the pole if $\epsilon > 0$. Direct integration produces the result

$$\Delta(\epsilon) = \langle j| - H_{\mathcal{Q}\mathcal{Q}} - \hat{\mathcal{Q}}V - V\hat{\mathcal{Q}}|j \rangle + \epsilon \langle j|\hat{\mathcal{Q}}|j \rangle + \pi \varkappa^2 \Theta(-\epsilon) \epsilon^l \sqrt{-\epsilon}, \quad (49)$$

and for imaginary part

$$\gamma_j(\epsilon) = 2\pi \varkappa_j^2 \Theta(\epsilon) \epsilon^{l+1/2}. \quad (50)$$

Here $\hat{\mathcal{Q}} = \int d\epsilon_j |j\epsilon_j\rangle \langle j\epsilon_j|$ is the projection operator into \mathcal{Q} space; Θ is the Heaviside step function. The first two terms in Eq. (49) appear as a correction to energy due to the possible non-orthogonality between the states of \mathcal{Q} and \mathcal{P} . They are small in any reasonably selected situation; they are identically zero in the examples shown below where

spaces \mathcal{P} and \mathcal{Q} are obtained from the full numerical solution of the Woods-Saxon potential. Only the second term in (49) depends linearly on energy.

The last term in Eq. (49) appears only below threshold and represents virtual excitation into continuum induced by interaction. This contribution is a continuous function of energy, that is also smooth except for the s -wave neutral particle decay channel. The behavior of the self energy $\Delta(\epsilon)$ including the s -wave $\sim \sqrt{\epsilon}$ type cusp is well studied in hadron physics, see also [33, 39]. The scaling coefficient a_j that enters this expression is typically small; the same coefficient determines the energy scaling of the decay width above threshold, Eq. (50), see Fig. 3. The behavior $\gamma \sim \epsilon^{l+1/2}$ is consistent with the phase-space volume for one-body decay. It is universal, so that, if the potential is being adjusted to reproduce a certain resonance energy, then the behavior of the width as a function of resonance energy remains the same [38, 39].

C. One-body channels in a many-body system

The one-body decay amplitude in a many-body system is given by the s.p. decay and the spectator overlap,

$$A_1^c(E) = a_j(\epsilon) \langle 1; N | b_j^\dagger | \alpha; N - 1 \rangle, \quad (51)$$

where energy of the continuum state is $E = E_\alpha + \epsilon$ and $c = \{\alpha, j\}$. This amplitude is to be directly used in the non-Hermitian effective Hamiltonian (10). Even on the level of s.p. decays, the approach outlined here goes beyond the consideration based solely on spectroscopic factors. Here the non-Hermitian part of the effective Hamiltonian is not a s.p. operator. Indeed, even s.p. decays can generate significant restructuring inside the nucleus. Effects, such as shape changes or changes in pairing coherence, are extremely important for the physics of nuclei far from stability. The energy dependence that was discussed earlier is another distinct feature.

Although in all calculations presented in this work we use a general form of the effective Hamiltonian, below we show a set of approximations that establish a correspondence with the traditional SM description of decay. For simplicity we assume that all internal s.p. states can be identified by spin and parity, i.e. the space is small enough not to include several major shells, so that there is no need in main quantum numbers. The non-Hermitian term in the full Hamiltonian coming from s.p. decay channels is then diagonal,

$$\langle 1 | W(E) | 2 \rangle = 2\pi\delta_{12} \sum_{c(\text{open})} |a_j(\epsilon_j)|^2 |\langle \alpha; N - 1 | b_j | 1; N \rangle|^2, \quad (52)$$

where s.p. energy satisfies $E = \epsilon_j + E_\alpha$; below we suppress the energy argument if it is unambiguous.

In the case of remote thresholds, the decay amplitudes become essentially independent of energy, and the set of continuum channels $c = \{\alpha, j\}$ includes almost all possible daughter states α . The completeness in α and energy independence can be then used to simplify (52),

$$\langle 1 | W | 2 \rangle = 2\pi\delta_{12} \sum_j |a_j|^2 \langle 1; N | b_j^\dagger b_j | 1; N \rangle. \quad (53)$$

As a result, W becomes a s.p. operator that assigns a width (36) to each s.p. state j coupled to continuum, $W = \sum_j \gamma_j b_j^\dagger b_j$. The same picture emerges when the residual SM interaction is weak. Then s.p. motion masters the dynamics, and the sum over daughter systems α in Eq. (52) is dominated by a single term. This again leads to Eq. (53) that is energy dependent, $W(E) = \sum_j \gamma_j(E) b_j^\dagger b_j$. The operator W here can be conveniently combined with the SM Hamiltonian just by introducing complex s.p. energies for unstable orbitals in the mean field (a simple instructive example was shown in [40]). Another point to be mentioned here is related to the treatment of the non-Hermitian part. In the full CSM diagonalization, virtual transitions to continuum and real decays influence the internal structure. This is particularly important at strong continuum coupling when coherence with respect to decay leads to the super-radiance phenomenon [7, 25, 41].

The second situation leading to the SM picture is the limit of weak continuum coupling when the matrix W can be treated perturbatively. In the lowest order, decays do not affect the internal state and we can solve the Hermitian problem first to obtain a many-body state $|\alpha\rangle$ with the width given by the expectation value

$$\Gamma_\alpha = \langle \alpha | W | \alpha \rangle = \gamma_j \Upsilon_j(\alpha). \quad (54)$$

This expresses a many-body decay width as a product of the s.p. width and the spectroscopic factor $\Upsilon_j(1) = \langle 1; N | b_j^\dagger b_j | 1; N \rangle$.

D. Two-nucleon emission

A two-body decay channel state is fixed by an $N - 2$ nucleus in its eigenstate α and a state of two nucleons in the continuum, Eq. (28). These states are characterized by total energy $E = E_\alpha + \epsilon_j + \epsilon_{j'}$ combined of the daughter energy E_α and energies of emitted nucleons in s.p. channels j and j' , total angular momentum and isospin of the emitted pair. Unless we are dealing with a bound two-particle continuum state, the channel, besides total energy E , has another continuous index describing the energy distribution between the particles.

As earlier, the two-body transition amplitude is generated by the matrix element $\langle 1|H|c; E\rangle$. Two different contributions can be identified as “direct” and “sequential”, Fig. 2. The defined above one-body part of the total Hamiltonian H cannot contribute to the direct decay vertex $1 \rightarrow \alpha + j + j'$. The two-body interaction responsible for this direct transition is discussed below. Even without two-body interactions, the “dressed” vertex is not zero since the $N - 2$ daughter state is a part of the virtual cloud of the $N - 1$ system to which one-body transitions are allowed. Such a second order perturbative sequential mechanism of decay is possible regardless of whether one-body channel is open or closed. Similar approach and classification of processes have been recently discussed in the context of two-proton radioactivity [42, 43] where on one hand the case is complicated by being a three-body Coulomb problem [44], while on the other hand extremely weak decays do not affect the internal nuclear structure allowing the use of the traditional real energy SM [43].

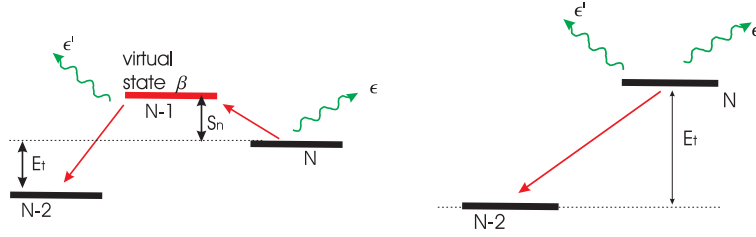


FIG. 2: (Color online) Diagrams for two-body decays, sequential (left part) and direct (right part).

1. Sequential decay

The dressed s.p. vertex for two-nucleon emission $\langle 1|H|c; E\rangle$ can be calculated with the help of Eq. (3) and solution (6),

$$A_1^c(E_c, E) = \sum_{\beta} \frac{A_1^{\{\beta j\}}(E_\beta + \epsilon, E) A_\beta^{\{\alpha j'\}}(E_\alpha + \epsilon', E_\beta)}{E_\beta - E_\alpha - \epsilon'} - \left(\{\epsilon, j\} \leftrightarrow \{\epsilon', j'\} \right). \quad (55)$$

Assuming that internal and external s.p. states are orthogonal and using one-body decay amplitude (51) for the second order process that takes place via a virtual state β being suppressed by the energy barrier, we obtain

$$A_1^c(E) = \sum_{\beta} a_j(\epsilon) a_{j'}(\epsilon') \left(\frac{\langle 1|b_j^\dagger|\beta\rangle \langle \beta|b_{j'}^\dagger|\alpha\rangle}{S_\beta + \epsilon} - \left(\{\epsilon, j\} \leftrightarrow \{\epsilon', j'\} \right) \right), \quad (56)$$

where we are considering only on-shell decay so that the initial state with energy $E = E_\alpha + \epsilon + \epsilon'$ undergoes a transition via the intermediate state with energy $E_\beta + \epsilon$. This is reflected in the denominator $S_\beta + \epsilon = E_\beta - E + \epsilon$, where S_β stands for separation energy from the intermediate system. Since c here contains a continuous index, the summation over channels is expressed as

$$\langle 1|W(E)|2\rangle = \pi \sum_{\alpha, j, j'} \int d\epsilon d\epsilon' \delta(E - E_\alpha - \epsilon - \epsilon') A_1^c(E) A_2^{c*}(E). \quad (57)$$

In order to avoid double counting due to fermion permutation we included a factor of 1/2 while making domain of integration symmetric. Eq. (57) may contain poles in open one-body channels corresponding to real states of an $N - 1$ system through which the two-body decay process can proceed. Such processes can be viewed as a second

order correction to the one-body decay via the daughter state β as a resonant state. Here we discuss only the off-shell contribution. An example of sequential decay is shown in Fig. 2.

The calculation of the non-Hermitian term W in the most general case was carried out numerically in the examples shown in the Sec. IV. Here we illustrate the case of a weakly decaying state $|\alpha_i\rangle$ when the decay width can be approximated by the diagonal element, $\Gamma = \langle\alpha_i|W|\alpha_i\rangle$. In this limit the problem is close to that of sequential decay discussed in [43, 45].

Taking into account the direct and exchange contributions to Eq. (56), assuming spherical symmetry and performing the summation over magnetic quantum numbers, we obtain two spectroscopic factors,

$$\Upsilon^d = \delta_{jj'}\delta_{\beta\beta'} \frac{|\langle\alpha_f||b_j||\beta\rangle\langle\beta||b_j||\alpha_i\rangle|^2}{(2\alpha_i+1)(2\beta+1)}, \quad (58)$$

and

$$\Upsilon^x = (-1)^{\beta+\beta'} \left\{ \begin{array}{ccc} \alpha_i & j & \beta' \\ \alpha_f & j' & \beta \end{array} \right\} \frac{\langle\alpha_f||b_{j'}||\beta'\rangle^* \langle\beta'||b_j||\alpha_i\rangle^* \langle\alpha_f||b_j||\beta\rangle \langle\beta||b_{j'}||\alpha_i\rangle}{2\alpha_i+1}, \quad (59)$$

where (and below) we use the Greek index of the many-body state as a symbol of angular momentum. The reduced matrix elements are defined as in [32]. The total width in the channel $|\alpha_i\rangle \rightarrow |\alpha_f\rangle$ is given by

$$\Gamma = \frac{1}{2\pi} \int d\epsilon d\epsilon' \delta(E_t - \epsilon - \epsilon') \sum_{\beta\beta'jj'} \gamma_j(\epsilon)\gamma_{j'}(\epsilon') \left(\frac{\Upsilon^d}{(S_\beta + \epsilon)^2} + \frac{\Upsilon^x}{(S_\beta + \epsilon')(S'_\beta + \epsilon)} \right) \quad (60)$$

As an illustration, we discuss a case of the $0^+ \rightarrow 0^+$ two-neutron decay. Here $\Upsilon^x = \Upsilon^d \equiv \Upsilon$, and we can view a full width as a sum of partial widths that depend on the final state α_f and intermediate state β . The characteristic energies in the problem are the one-neutron separation energy to the state β , $S_\beta = E_\beta - E_{\alpha_i}$, and two-neutron decay energy, $E_t = E_{\alpha_i} - E_{\alpha_f}$ (minus two-neutron separation energy). We assume the situation with small available energy $E_t = \epsilon + \epsilon'$, when the energy scaling of the s.p. decay widths, $\gamma_j = 2\pi|a^j(\epsilon)|^2 \sim \epsilon^{l+1/2}$, can be used. Introducing $q = E_t/S_\beta$ we obtain

$$\Gamma_{\beta}(0 \rightarrow 0) = \Upsilon \frac{\gamma_l(E_t)\gamma_{l'}(E_t)E_t}{S_\beta^2} \mathcal{B}_{ll'}(q), \quad (61)$$

which includes the phase space integral

$$\mathcal{B}_{ll'}(q) = \frac{(2+q)}{2\pi} \int_0^1 \frac{x^{l+1/2}(1-x)^{l'+1/2}}{(1+qx)^2[1+q(1-x)]} dx. \quad (62)$$

In the limit $S_n \gg E_t$ we obtain $\mathcal{B}_{ll'}(q) = B(l+3/2, l'+3/2)/\pi$, where $B(x, y)$ is a beta function. The decay rate is suppressed by the energy denominator $1/S_\beta^2$. The two-body decay width scales with energy as E_t^2 . This is consistent with the phase space volume estimate, $\Gamma \sim \delta^3(P_t - P)\delta(E_t - E) \prod_i (d^3k_i/\epsilon_i)$, where P is total momentum and the product \prod_i runs over the fragment indices including the daughter nucleus. For the isotropic case integrated over all angles, the width is proportional to $\gamma \sim k \sim E_t^{1/2}$ in one-body decay; the same assumptions lead to $\Gamma \sim E_t^2$ for the two-body decay (three-body final phase space).

In the opposite limit, $S_n \ll E_t$ or $q \rightarrow \infty$, we have $\mathcal{B}_{ll'}(q) = B(l-1/2, l'+1/2)/(2\pi q^2)$. This expression diverges for an s -wave. The exact integration in the s -wave case gives

$$\Gamma_{\beta=1/2}(0 \rightarrow 0) = \frac{\gamma_0^2(E_t)\Upsilon_\beta E_t}{4(2S_\beta + E_t) \sqrt{S_\beta(S_\beta + E_t)}}. \quad (63)$$

Note the divergence in the s -wave channel when separation energy goes to zero. The s -wave state in the intermediate nucleus β is so broad that even being slightly higher in energy it still poses no barrier for the sequential decay. The generic behavior of the isotropic decay width as a function of energy can be traced from Eq. (63), where $\Gamma \sim E_t^2$ if energy is low, $E_t \ll S_\beta$, but once energy is getting above S_β the behavior changes to $\Gamma \sim \sqrt{E_t}$. This shows that the presence of the one-body resonance changes the nature of sequential decay reflecting the one-body phase space characteristics.

2. Direct decay

Direct two-body transitions are generated by the two-body part of the Hamiltonian $H_{\mathcal{P}\mathcal{Q}}$ that takes a nucleon pair coupled to angular momentum L , $p_L = [b_j b_{j'}]_L$, from internal space \mathcal{P} and transfers it to the two-body continuum \mathcal{Q} , see the right part in Fig 2. The transition amplitude has a generic form,

$$A_1^c(E) = a^{(j_1 j_2)}(\epsilon_1, \epsilon_2) \langle 1; N | \left(p_L^{(j j')} \right)^\dagger | \alpha; N - 2 \rangle, \quad (64)$$

where a direct two-body transition amplitude, $a^{(j_1 j_2)}(\epsilon_1, \epsilon_2)$, is introduced (not to be confused with s.p. amplitudes $a^j(\epsilon)$). This amplitude can be calculated for a given two-body interaction. For example, assuming for simplicity a coordinate form $V^{(2)}(r, r')$, where r and r' are particle coordinates in the mean-field frame, the amplitude can be expressed following the definition of Eq. (7) and normalized free particle states F_j as

$$a^{(j_1 j_2)}(\epsilon_1 \epsilon_2) = \langle j_1 j_2 | V^{(2)} | j_1, \epsilon_1; j_2, \epsilon_2 \rangle = \frac{2\mu}{\pi \sqrt{k_1 k_2}} \int_0^\infty dr dr' F_{j_1}(r) F_{j_2}(r') V^{(2)}(r, r') u_{j_1}(r) u_{j_2}(r'). \quad (65)$$

The low-energy behavior of the direct amplitude can be understood without specification of the residual interaction by taking into consideration the long wavelength behavior of the Bessel functions associated with the regular solution, $F_l(r) \sim (kr)^{l+1}$ at $k \rightarrow 0$. The decay rate can be estimated by integration over continuous channel variables as in (57),

$$\Gamma \sim \int \left| a^{(j_1 j_2)}(\epsilon_1 \epsilon_2) \right|^2 \delta(E_t - \epsilon_1 - \epsilon_2) d\epsilon_1 d\epsilon_2 \sim E_t^{l_1 + l_2 + 2}. \quad (66)$$

The same answer as the one obtained for the sequential transition reflects the nature of three-body final phase space. The direct transition however is not suppressed by the one-body energy barrier and is not related to decay amplitudes for one-body decays.

We conclude the discussion of two-body decay processes with the word of caution: the full amplitude in a given decay channel is the sum of the direct and sequential contributions and the observed width or cross section carries their interference.

IV. APPLICATIONS

A. How the method works

Before turning to the discussion of the specific results we outline the stages involved in the calculation. A special feature of our approach is the exact treatment of threshold behavior. This requires the knowledge of the topography of thresholds and therefore has to rely on the preceding solution for the daughter systems. In this way we come to problems of considering the daughter chains in their entirety. Thus, except for the case of the traditional SM, where the Hermitian Hamiltonian matrix is diagonalized separately for each nucleus, in all calculations the nuclides (in our examples below the isotopes) are coupled by the decay chains.

The procedure starts from the closed core (specifically, ${}^4\text{He}$ or ${}^{16}\text{O}$) and continues toward heavier isotopes so that the properties of all possible daughter nuclei are known prior to each new calculation. The process of calculating resonant states is iterative. We start with a given state obtained from the conventional SM. For this state we review all possible decays, including the two-body ones. By conducting scattering calculations at relevant energy or via appropriate power-law dependence of Eq. (50) at low energies and including the spectroscopic factors from structural rearrangement of spectator nucleons we determine the contributions from each decay channel to the non-Hermitian term W . The diagonalization of the full Hamiltonian with the non-Hermitian part results in the next iteration for energy and width of the state under consideration. For each resonant state this process continues until convergence is reached. The Breit-Wigner definition of resonances is used so that scattering calculations are done at real energy.

By construction of the model, with $\Delta(E)$, Eq. (11), assumed to be included in the adjusted SM Hamiltonian with neglected energy dependence, bound levels coincide with those in the standard SM. For unbound states, this choice makes our internal propagator equivalent to the R -matrix used in spectroscopic analysis of experimental data. Therefore this design is most suitable for the effective extraction of interaction parameters from experiment.

The continuum coupling restructures internal states, and energies of resonances above the decay threshold deviate from the SM predictions. For narrow states and well separated resonances, the resulting effect is small. The spherical shape of the semi-magic system is stable; in addition, strong collective pairing reduces the effect of decays onto internal

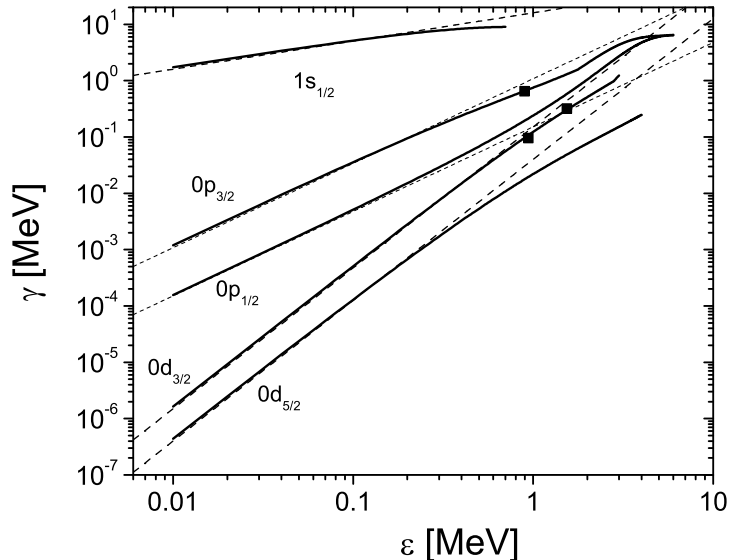


FIG. 3: Single-particle decay width as a function of resonance energy for the p and sd shell models. The solid lines represent results of the reaction calculations based on the Woods-Saxon potential appropriate for the corresponding case (helium or oxygen) discussed in text. One experimental point on the p -state corresponds to the ground state $3/2^-$ resonance in ${}^5\text{He}$ ($\epsilon = 0.895$ MeV and $\gamma = 648$ keV). Two points for the d -state correspond to experimentally known $3/2^+$ resonances in ${}^{17}\text{O}$ ($\epsilon = 0.941$ MeV and $\gamma = 98 \pm 5$ keV) and ${}^{19}\text{O}$ ($\epsilon = 1.540$ MeV and $\gamma = 320 \pm 25$ keV [58]). The near-threshold power law fits of Eq. (50) are shown with dashed lines.

structure in these particular examples. Whence, for s.p. decays, the case (a) in Table I, the use of the spectroscopic factor approximation discussed in Sec. III C is rather good. Here we are far from strong coupling to continuum [12, 25, 53, 54] that may cause an internal phase transition with formation of broad (super-radiant) and very narrow (trapped) states. In nuclear physics this phenomenon separates compound and direct reactions [25, 55, 56]. A trace of this effect is seen in Table I, where decaying states have their resonant energy shifted from SM prediction, the lowest states of given quantum numbers are pushed into continuum [7].

The cross section calculations follow directly the formalism outlined in Sec. II B. The large scale repetitive matrix inversion and instability in the vicinity of the poles presents a significant technical challenge. In this work we employed a new numerical method that expands the unperturbed propagator (16) in the time domain using Chebyshev polynomials. The entire procedure is similar to the Lanczos technique and involves only matrix vector multiplication - a fast operation with sparse matrices. The resulting R matrix is then used in the Woodbury equation (18) leading to a full propagator and scattering cross section.

B. Helium isotopes

For the chain of helium isotopes from ${}^4\text{He}$ to ${}^{10}\text{He}$, the results are summarized in Table. I. The internal valence \mathcal{P} -space contains two s.p. levels, $p_{3/2}$ and $p_{1/2}$, the α -particle core is kept inert. The effective interaction within this model space and s.p. energies are borrowed from [46, 47]. Without additional terms, this would be merely a conventional SM leading to the bound states that are listed as E(SM) in Table I.

The one-body part of the coupling Hamiltonian $H_{\mathcal{P}\mathcal{Q}}$ is defined using the Woods-Saxon potential. However, at low energies the s.p. decay widths can be well approximated by near-threshold dependence of Eq. (41) as $\gamma_{3/2}(\epsilon) = 1.08 \epsilon^{3/2}$ MeV and $\gamma_{1/2}(\epsilon) = 0.151 \epsilon^{3/2}$ MeV for $p_{3/2}$ and $p_{1/2}$ states, respectively, see Fig. 3. The results of calculation limited to s.p. decays are shown as case (a) in Table I. The ‘‘Borromean’’ ${}^6\text{He}$ nucleus requires two-body decays. The sequential two-body decay as a second order process built on the one-body amplitudes involves no additional parameters. This process is included in the results shown as case (b) in Table I.

A	J	E(SM)	E(a)	E (b)	E(CSM)	E(EX)	$\Gamma(a)$	$\Gamma(b)$	$\Gamma(\text{CSM})$	$\Gamma(\text{EX})$
4	0	0	0	0	0	0	0	0	0	0
5	3/2	0.992	0.992	0.992	0.992	0.895	0.6	0.6	0.6	0.648
5	1/2	4.932	4.932	4.932	4.932	4.895	4	4	4	4.1
6	0	-1.379	-1.379	-1.379	-1.379	-0.973	0	0	0	0
6	2	0.515	0.515	0.529	0.529	0.825	0	0.248	0.248	0.113
6	2	4.745	5.25	5.25	5.25		2.566	2.566	2.566	
6	1	5.889	5.32	5.32	5.32		0.922	0.922	0.922	
6	0	11.088	10.911	10.911	10.803		5.532	5.532	12.303	broad
7	3/2	-1.016	-1.016	-1.016	-1.016	-0.528	0.046	0.046	0.046	0.15
7	1/2	2.24	2.239	2.253	2.253	2.172	2.357	2.689	2.69	3
7	5/2	2.85	2.888	2.911	2.911	2.393	0.727	0.944	0.944	1.99
7	3/2	4.495	4.379	4.222	4.22	(5.273)	0.541	1.113	1.246	(4)
7	3/2	10.223	8.857	9.521	9.544		7.818	16.379	21.578	
8	0	-3.591	-3.591	-3.591	-3.591	-3.108	0	0	0	0
8	2	0.19	0.196	0.191	0.19	-0.308	0.231	0.506	0.53	
8	1	2.427	2.304	2.331	2.321		1.026	1.455	1.418	
8	0	6.376	6.003	6.527	6.489		5.286	3.456	15.449	
8	2	6.882	6.839	6.538	6.572		2.283	13.86	14.94	
9	1/2	-1.992	-1.992	-1.992	-1.992	-1.958	0.634	0.634	0.634	0.1
9	3/2	2.805	2.801	2.802	2.797	-0.6	1.557	2.425	2.443	0.8
10	0	-1.649	-1.649	-1.649	-1.649		0.073	0.504	0.746	0.3

TABLE I: Comparison of conventional SM and CSM with data for He isotopes (all numbers in MeV; energies are measured from the ground state of ${}^4\text{He}$). The first two columns indicate the mass number and spin of the state. The next five columns compare energies as follows: $E(\text{SM})$ - traditional shell model; $E(a)$ - CSM with only one-body decays included; $E(b)$ - CSM with one-body decay and its second order contribution to the two-body process; $E(\text{CSM})$ - full CSM including the direct two-body decay mode; $E(\text{EX})$ - experimental data (some of them have large uncertainties and depend on the way of analysis). Last columns compare decay widths from CSM calculations with data [50, 51, 52]; the SM calculation gives only discrete energies.

The judgment about the direct two-body decays, their importance, and whether two-body terms have to be included in $H_{\mathcal{P}\mathcal{Q}}$ can be made with comparison of theory versus experimental data. Considering the simplest two-body case of ${}^6\text{He}$ we observe that the included sequential decay provides a reasonable description for the lowest 2_1^+ resonance in ${}^6\text{He}$. However, the need to include direct two-body decay comes from consideration of a broad asymmetric resonance structure at excitation energy $\sim 3 - 15$ MeV [48, 49] ascribed to neutron skin oscillations. Although an experimental controversy exists in relation to this structure, our results below, as well as earlier studies, see [48], suggest a direct two-body breakup process. Based on the experimental exclusion of 2_2^+ possibility by [49], we tentatively identify this resonance as a spin zero pair-vibration excitation generated by a coherent transition of the $L = 0$ neutron pair between the two s.p. orbitals and introduce direct two-body decay with the pair emission in the $L = 0$ channel. At this level of experimental precision and with the sequential decays being already included, there is no compelling evidence for direct decays in other angular momentum channels.

Without introducing a specific isotropic form of the two-body interaction for $H_{\mathcal{P}\mathcal{Q}}$ we adopt a low-energy “pairing” approximation assuming that all $L = 0$ neutron pairs couple to continuum with the same amplitude $a^{(L=0)}(\epsilon_1, \epsilon_2) = (\epsilon_1 + \epsilon_2)/3\sqrt{2\pi}$. The numerical constant here sets the strength of the residual two-body interaction. This is the only parameter of the model, and with limited experimental knowledge it was selected to roughly reproduce the broad resonant structure in ${}^6\text{He}$. The results of the full calculation are shown in Fig. 4 and listed as (CSM) in Table I. Fig. 4 also shows elastic neutron scattering cross section from the ground state of the $N - 1$ nucleus in $M = 0$ (even) or $M = 1/2$ (odd mass) magnetic moment state. The cross section is computed with the same CSM parameters but within the case (a) discussed above.

Below we comment on some of the features of the results.

(i) The ground states of ${}^4,6,8\text{He}$ are nucleon-stable in agreement with experiment.

(ii) The results reveal information about structure and dominant decay modes. For example, for the ${}^7\text{He}$ isotope, that has not been used for an adjustment of interactions, they agree with recent experiments [51, 52]. Our results support the “unusual structure” of the $5/2^-$ state identified by [52]. Due to its relatively high spin, this state, unlike the neighboring $1/2^-$ state, decays mainly to the 2^+ excited state in ${}^6\text{He}$. Concerning the deviations from the data in the width of this state and $3/2^-$ state, we may comment that experimentally [52], although there are still serious uncertainties, it is most likely that the contribution from the triple decay sequence, sequential two-body followed by one-body, is important for the lifetime of the $3/2^-$ state. The processes of the third order one-body decay or second order combination of direct two-body followed by one-body, are not included in this calculation but in light of the experimental data they should be considered in the future.

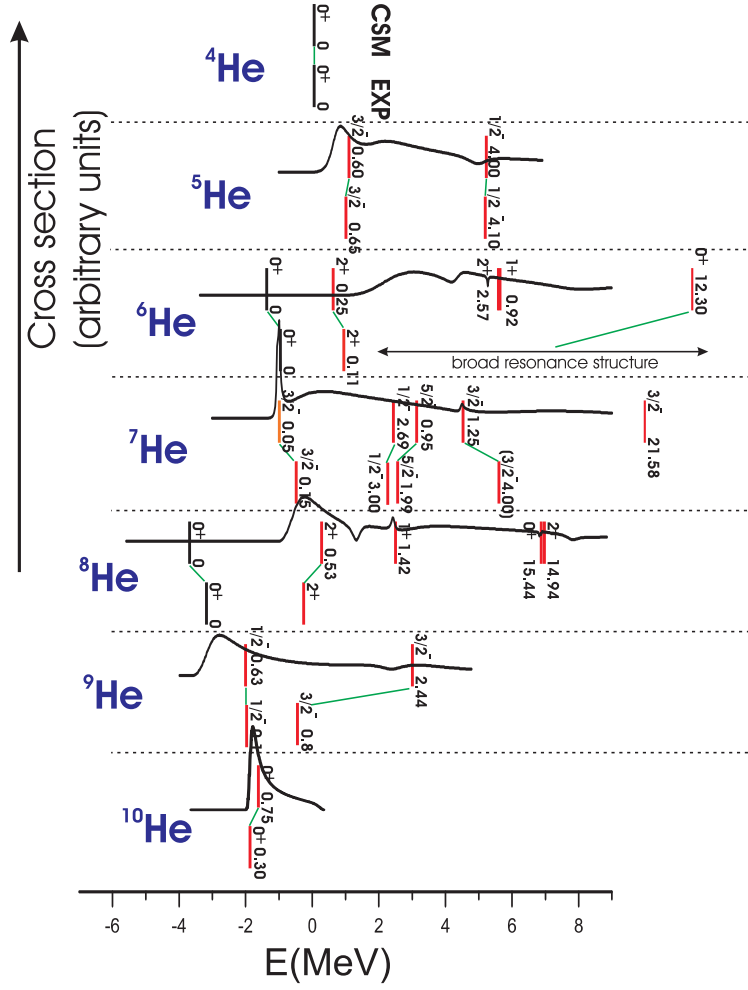


FIG. 4: (Color online) CSM results for He isotopes. The states in the chain of isotopes starting from ${}^4\text{He}$ (top) to ${}^{10}\text{He}$ (bottom) are shown as a function of the energy relative to ${}^4\text{He}$. The horizontal dotted lines separate each isotope and for each case states from CSM are shown above experimentally observed states. The decay width (in MeV) is shown for each state along with spin and parity. The solid lines above CSM states shows the elastic neutron scattering cross section from the spin polarized state of $N - 1$ isotope, see text for details.

(iii) Our results and, most importantly, the theoretical interpretation of the role that one-body and two-body interaction terms play in the dynamics of decay agree with earlier findings in [19] where a different method involving a full diagonalization without separation of continuum into channels was used.

(iv) For the heaviest isotopes and, in particular, for the discussion of the presently interesting case of ${}^9\text{He}$, the extension to the sd shell is necessary.

(vii) The scattering cross section is non-zero only above the thresholds (the ground state of the $A - 1$ nucleus). Cross section curves are generally not symmetric and have neither Gaussian nor Lorentzian shape. For low-lying states with the width big enough to reach threshold, the distortion is particularly noticeable.

(viii) For broad resonances, the identification of resonances (or poles of the scattering matrix) with a peak in the cross section is ambiguous. Interference between different resonances, including rather remote once, is significant in

A	j	mode	EXP	Q	Γ	theory	E	Q	Γ
17	$3/2^+$	γn	5.085	0.941	96	WS	4.5	1.0	122
18	2^+	$\gamma \alpha n$	8.213	0.169	1 ± 0.8	USD	9.465	1.242	200
18	1^+	αn	8.817	0.773	70 ± 12	USD	10.823	2.600	85
18	4^+	$\gamma \alpha n$	8.955	0.911	43 ± 3	USD	8.750	0.526	28
19	$5/2^+$	n	5.148	1.191	3.4 ± 1	USD	5.011	1.121	5.1
19	$9/2^+$		5.384	1.427	~ 0	USD	5.175	1.282	0
19	$3/2^+$	n	5.54	1.58	320	USD	5.529	1.636	290
19	$7/2^+$	n	6.466	2.509	small	USD	6.880	0.808 ^a	63
24	2^+	n	?	?	?	HBUSD	4.850	0.489	18
26	0^+	$2n$	0	?	?	HBUSD	0	0.021	0.02
28	0^+	$2n$	0	?	?	HBUSD	0	0.345	14

^athe Q -value is measured for the excited state in daughter system.

TABLE II: Lowest resonance states in the chain of oxygen isotopes. The experimental data on the left, (EXP) - energy of the state (MeV), Q - energy above threshold (MeV), Γ - width (keV), are compared to the theoretical results on the right. The decay mode in the second column indicates the decay branches assumed by experimentalists [50, 60].

this case.

C. Oxygen isotopes

The internal space here is represented by the $s_{1/2}$, $d_{3/2}$ and $d_{5/2}$ s.p. orbitals composing the usual sd -shell model. The standard SM interactions (USD [30] or its slightly modified version for heavier isotopes HBUSD [57]) were used in these calculations.

Since we use the Woods-Saxon potential for reaction calculations, it is important to make sure that the potential create proper resonant states. For few low-lying s.p. resonances with large spectroscopic factors, we adjust the depth of the potential so that the correct s.p. resonance energy is indeed ensured. The Woods-Saxon potential parameterization with the mass dependent depth [58, 59] was demonstrated to reproduce the s.p. resonances and bound states with good precision for nuclei around mass $A = 16$. For the majority of high-lying states, the potential is not readjusted, here the decay amplitude is computed directly from Eq. (34). The resonance phenomenon in this case is due to the many-body effect where the complexity of the many-body states makes the overlap in Eq. (51) small.

In Fig. 3 the widths of the resonant states $s_{1/2}$, $d_{3/2}$ and $d_{5/2}$ are shown as a function of their energy being found with the aid of the Woods-Saxon potential with variable depth. The curves are limited to the near-threshold region approximately determined as $kR < l$ (and $kR \ll 1$ for $l = 0$) where R is the nuclear radius. For oxygen, this limits the d -wave at about 3 MeV. The curves are close to straight lines displaying the appropriate power law scaling (50) of the decay width as a function of energy. The lines can be fit by equations (with ϵ in units of MeV) $\gamma(s_{1/2}) = 16\epsilon^{1/2}$, $\gamma(d_{3/2}) = 0.15\epsilon^{5/2}$, and $\gamma(d_{5/2}) = 0.04\epsilon^{5/2}$. These fits are shown with dashed lines.

In Fig. 5 we show an overview of the full CSM calculation for oxygen isotopes within the sd shell. Some of the first results were reported earlier [7, 8].

Our calculations are in a good agreement with available experimental data for the oxygen isotopes [50, 60]. One has to emphasize again that, with the assumption of the self energy term Δ being a part of the conventional SM Hamiltonian, the bound states are exactly the same as obtained in the usual SM calculation. The novelty appears when the states above decay thresholds are considered. The properties of a few experimentally identified resonances in oxygen isotopes are compared to the CSM predictions in Table II.

There are two cases in ^{17}O and ^{19}O corresponding to the neutron emission from the $d_{3/2}$ orbital. These rather pure s.p. decays involve little many-body physics and are well described with the Woods-Saxon potential model, Fig. 3. Here the SM may be used to predict the neutron decay energy, however there is an obvious improvement if the experimental Q -value is used in the s.p. reaction calculations. The power law for the energy dependence of the decay width can enhance the predictive power of the description.

The two-body case of ^{18}O is more complicated, however there are only 14 states in the sd shell model. The comparison of the level structure and neutron scattering cross section with data is shown in Fig. 6. The SM below neutron decay threshold (zero on the plot) is in an impressive agreement with the data. Here, for all sd SM states shown with longer ticks (in red, color online), the experimental counterpart can be easily identified in the observed spectrum. Practically all remaining observed negative parity states below neutron threshold can be identified with particle-hole excitations using an extended $p - sd - pf$ SM. In theoretical calculation, these states are shown with

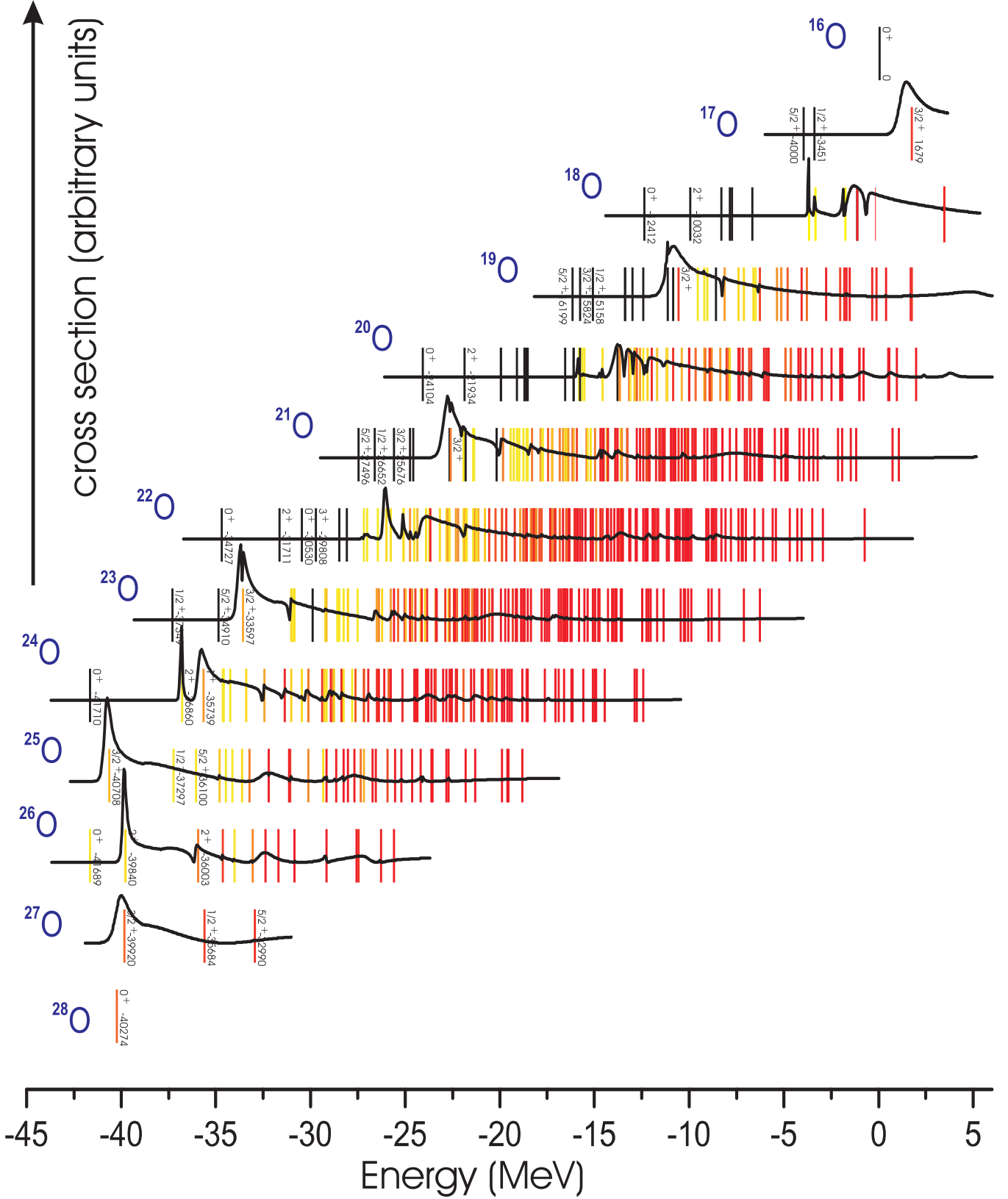


FIG. 5: (Color online) CSM calculation for oxygen isotopes with the HBUSD interaction. The states (vertical bars) are plotted as a function of absolute energy computed relative to ground state ^{16}O . States shown with solid black lines are stable in our model; they are either below decay thresholds or with decays forbidden due to the angular momentum restrictions in the selected valence space. States from yellow (color online)/lighter shade of gray (long lifetime) to red/darker gray (short lifetime) are resonance states. For some of the low-lying states the energy (in units of keV), spin and parity are given. Along with the resonant level structure above thresholds, the elastic d -wave neutron scattering cross section, off a ground state of a daughter nucleus with $M = 0$ (even mass) or $M = 1/2$ (odd mass) magnetic quantum number, is plotted as a function of energy. The cross section is obtained as a part of the same CSM calculation.

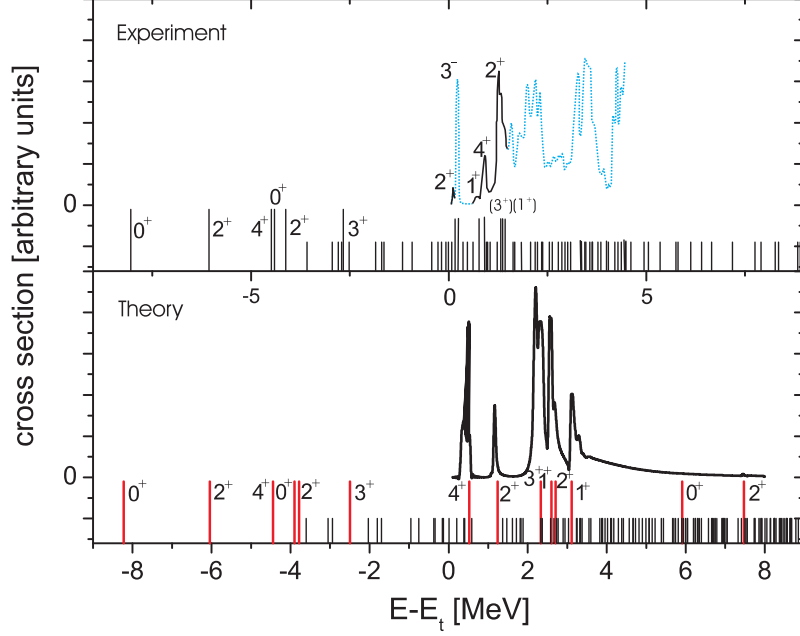


FIG. 6: (Color online) The lower panel is the result of the CSM calculation of the level structure and neutron scattering cross section from the ground state of ^{17}O . Marked levels corresponding to the sd -shell model states are included in CSM calculation. All other levels result from the expanded $sd - pf$ shell calculation (see text); the configurations of this type are not coupled to continuum and corresponding (negative parity) states do not appear in the cross section plot. The upper panel corresponds to the empirical level scheme in ^{18}O . The neutron scattering cross section on the upper panel is indirectly inferred from the $^{14}\text{C}(\alpha n)^{17}\text{O}$ reaction [61] and other compilations [60, 62, 63]. The parts of the cross section shown with solid line are expected to be dominated by the positive parity $l = 0$ or $l = 2$ partial waves and thus can be distantly juxtaposed to the curve on the lower plot.

small lines (the WBP cross-shell interaction from Ref. [31] was used).

Due to the resonant nature of states, the experimental picture above neutron decay threshold becomes more ambiguous. The lowest near-threshold state 2^+ may correspond to one of the higher-lying 2^+ states in our model, see Fig. 6 and Table II. Due to the significant difference in energy above threshold between this state and its possible theoretical counterpart, comparison of the decay widths is inappropriate. Following this state, there are rather narrow 4^+ and 1^+ states (the experimental assignment of 1^+ for the latter state is still uncertain), see Table II and Fig. 6. Although in theoretical calculation these states appear in a different order their observed and calculated widths appear to agree. Beyond this point there are several broad 100-200 keV unidentified resonances observed in experiment. They may be juxtaposed to 150-400 keV wide 2^+ , 3^+ , and 1^+ states appearing in the CSM calculation. To support this argument, we show on the lower panel of Fig. 6 the CSM neutron scattering cross section computed using Eq. (14). Since this calculation takes into account only $l = 0$ and $l = 2$ partial waves, the peaks from negative parity states do not appear. On the upper plot we roughly reproduce the experimental cross section obtained from indirect reactions, Refs. [60, 61, 62, 63]. The portion of the curve corresponding to positive parity resonances that are expected to be present in the theoretical calculation is shown by the solid black curve. There is a reasonable similarity in the resonant structure corresponding to the set of wide states 2^+ , 3^+ , and 1^+ . In the experiment, the spin-parity assignments for the states shown in Fig. 6 in brackets have not yet been confirmed.

The cross section picture indicates that our interpretation is plausible, while differences, by the factor of 2 to 4, in the resonance parameters may be due to different definitions of the width used in the data analysis. The broadness of these resonances causing difficulties in experimental analysis and interpretation of peaks is here a trivial consequence of the simple two-particle structure of ^{18}O that implies high spectroscopic factors for s.p. decay. The situation changes in the next isotope ^{19}O where there is only one broad s.p. $3/2^+$ state that stands out in the calculations of the cross section. The majority of other states are narrow due to the many-body complexity. They would not be visible on the plot of the cross section; on the other hand, this allows for the direct comparison of widths and energies shown in Table II. The level scheme inferred from experiments with ^{19}O fits well the overall picture of oxygen isotopes as

shown in the insert of Fig. 3.

Only little is known about the heavier oxygen isotopes although the situation is going to change in the near future with the new radioactive beam experiments. In Table II we quote some, in our view the most interesting, predictions of the model. The cases of ^{26}O and ^{28}O are just beyond the drip line. The ground states of these nuclei are unstable with respect to the neutron pair emission. Sec. III D, while being centered around interactions, discussed how to tackle such cases. Unfortunately, the uncertainty in the effective interactions complicates the job of predicting. We have no firm knowledge about the interaction coupling internal states to the continuum and, unlike the helium case, in the oxygen data we could not find a case to determine this coupling phenomenologically. Thus we only consider here the case of sequential decay driven by what we believe to be a well defined one-body potential.

The second problem is that the traditional SM adjusted to experimental data near the stability line cannot be extrapolated with full certainty to the vicinity of drip lines. The role of the self-energy term $\Delta(E)$ is another question. Indeed, the well established USD interaction predicts ^{26}O to be bound which is known from experiments not to be the case. In our calculations we had to resort to the HBUSD interaction specifically adjusted to heavier isotopes. The Q -value coming from this interaction in the case of ^{26}O is only 21 keV while the typical SM uncertainty in level energies is about 200 keV. This uncertainty entering the power law scaling of decay width versus energy makes the lifetime predictions unreliable.

Thus, while collecting our calculations in Table II we see our strongest prediction through Eq. (63). In both cases of ^{24}O and ^{26}O , the lowest $3/2^+$, $1/2^+$ and $5/2^+$ states in the adjacent isotopes ^{23}O and ^{25}O are the main candidates for the intermediate states involved in the sequential two-body decay. This is because of the low energy barrier in combination with large spectroscopic factors of these mainly s.p. states. At the same time, in the case of ^{24}O we have separation energies $S_{3/2} = 0.98$, $S_{1/2} = 4.39$ and $S_{5/2} = 5.54$ MeV; the corresponding spectroscopic factors are $\Upsilon_{3/2} = 0.28$, $\Upsilon_{1/2} = 0.019$ and $\Upsilon_{5/2} = 2.2 \times 10^{-4}$. In addition to spectroscopic information, the kinematics of the phase-space volume is another essential factor. A simple estimate with the aid of Eq. (63) shows that the transition through the s -state would dominate throughout the entire region below s.p. threshold. Due to level energetics, two-body decay remains significant even in the presence of the open one-body channel. However, the simple power law scaling used to obtain the phase space integrals Eq. (62) may no longer be valid high above threshold. If the ground state in ^{24}O were at $E_t = 1$ MeV above two-neutron decay threshold, while still right at the opening of one-neutron decay channel into the $3/2^+$ state of ^{23}O , $S_{3/2} = 0$, the decay width coming from sequential decay would be about 30 keV, as opposed to 20 eV in Table II quoted for $E_t = 0.021$ MeV.

V. CONCLUSION

The first goal of this work is to present a systematic and detailed discussion of the continuum shell model as a step in the direction of unifying the nuclear structure with nuclear reactions. We amplify and extend the ideas and methods started in our earlier works [7, 8]. In this presentation we clarify the CSM formalism and show its relation to the standard SM. One of the important points of this work was physical interpretation of various results. On the shell model side, we highlighted the meaning of solutions of the energy-dependent non-Hermitian effective Hamiltonian and identified the procedures to be taken in relation to different definitions of resonant states. On the reaction side, we show how the scattering matrix, cross sections and related quantities can be calculated; the unitarity properties of the scattering matrix built in the model are emphasized.

The general discussion of s.p. decays centers around the potential s.p. problem. This textbook problem is not only a central part of calculations but it also provides an important parallel to the full CSM description. Here the Gamow states, decay amplitudes and scattering matrix can be calculated through numerical solutions of the Schrödinger equation in coordinate space. This allows one to establish a transparent relation and interpretation of the same quantities in the full CSM.

The consideration of two-body decays is one of the significant advances of the present formulation. Considering the one- and two-body terms in the part of the Hamiltonian that links the internal shell model and external reaction space we get keys to the sequential and direct decays, respectively. In the case of sequential decay, a second order one-body process, we discuss the transition through the resonance tail, namely the role of broad one-body resonances located in the intermediate nucleus above threshold. The direct, or correlated, decay processes are strongly related to the problem of pairing and other coherent effects in the continuum. This problem, important also for physics of neutron stars, is still far from being solved.

The last section of this work shows practical applications of the model. The self-consistency in energy, proper open channels and realistic reaction calculations, parent-daughter structure relations through the decay chain, – are discussed as the essential elements of the model. The diagonalization of the full Hamiltonian with both Hermitian and non-Hermitian parts is emphasized as an important component for treating properly the mutual influence of structure and reactions. The discussion of the extreme effects of this nature, such as super-radiance, is outside the scope of this

paper, see [25, 53, 54].

Another goal of this work is to report the advance in practical applications of the CSM and in particular to demonstrate new cross section calculations performed in the same unified framework and presented along with the bound states and resonance parameterizations. Comparison with experimental data indicates a satisfactory agreement for both helium and oxygen isotopes. The possible role of sequential decay in heavy oxygen isotopes is discussed and predictions for the decay width are given. Coming experimental data will be instrumental for further development of theory.

We did not discuss here the computational problems which are of a higher level of difficulty compared to the normal SM. In fact, the novel methods for constructing Green's functions for large-scale calculations using the Chebyshev polynomial expansion and Woodbury equation stand behind the presented results. However, the technical and numerical details are outside the scope of this article; they will be presented elsewhere. From the conceptual viewpoint, the basic question of effective interactions remains unsolved. We used here a semi-empirical method of combining the SM experience with finding the missing cross-space matrix elements from the solution of the scattering problem and numerical fits based on general requirements of quantum-mechanical threshold behavior. The inclusion of giant resonances, more complicated decay modes and cluster channels is also on the agenda for future work.

Acknowledgments

The authors acknowledge support from the U. S. Department of Energy, grant DE-FG02-92ER40750; Florida State University FYAP award for 2004, and National Science Foundation, grants PHY-0070911 and PHY-0244453. Help and useful discussions with B.A. Brown and G. Rogachev are highly appreciated.

-
- [1] V. Zelevinsky, ed., *Nuclei and Mesoscopic Physics*, vol. 777 of *Conference Proceedings* (AIP, 2005).
 - [2] B.A. Brown, *Prog. Part. Nucl. Phys.* **47**, 517 (2001).
 - [3] J. Fridmann *et al.*, *Nature* **7044**, 922 (2005).
 - [4] P. Hansen and B. Sherrill, *Nucl. Phys.* **A693**, 133 (2001).
 - [5] E. Caurier, G. Martinez-Pinedo, F. Nowacki, A. Poves, and A. P. Zuker, *Rev. Mod. Phys.* **77**, 427 (2005).
 - [6] C. Mahaux and H. Weidenmüller, *Shell-Model Approach to Nuclear Reactions* (North-Holland, Amsterdam, 1969).
 - [7] A. Volya and V. Zelevinsky, *Phys. Rev. C* **67**, 54322 (2003).
 - [8] A. Volya and V. Zelevinsky, *Phys. Rev. Lett.* **94**, 052501 (2005).
 - [9] H. Feshbach, *Ann. Phys.* **5**, 357 (1958).
 - [10] H. Feshbach, *Ann. Phys.* **19**, 287 (1962).
 - [11] I. Rotter, *Rep. Prog. Phys.* **54**, 635 (1991).
 - [12] I. Rotter, *Phys. Rev. E* **64**, 036213 (2001).
 - [13] V. Weisskopf and E. Wigner, *Z. Phys.* **63**, 54 (1930).
 - [14] O. Rice, *J. Chem. Phys.* **1**, 375 (1933).
 - [15] U. Fano, *Nuovo Cim.* **12**, 156 (1935).
 - [16] U. Fano, *Phys. Rev.* **124**, 1866 (1961).
 - [17] R. Id Betan, R. J. Liotta, N. Sandulescu, and T. Vertse, *Phys. Rev. Lett.* **89**, 042501 (2002).
 - [18] N. Michel, W. Nazarewicz, M. Ploszajczak, and K. Bennaceur, *Phys. Rev. Lett.* **89**, 042502 (2002).
 - [19] N. Michel, W. Nazarewicz, M. Ploszajczak, and J. Okolowicz, *Phys. Rev. C* **67**, 054311 (2003).
 - [20] N. Michel, W. Nazarewicz, and M. Ploszajczak, *Phys. Rev. C* **70**, 064313 (2004).
 - [21] J. Okolowicz, M. Ploszajczak, and I. Rotter, *Phys. Rep.* **374**, 271 (2003).
 - [22] G. Hagen, M. Hjorth-Jensen, and J.S. Vaagen, *Phys. Rev. C* **71**, 044314 (2005).
 - [23] C.A. Engelbrecht and H.A. Weidenmüller, *Phys. Rev. C* **8**, 859 (1973).
 - [24] L. Durand, *Phys. Rev. D* **14**, 3174 (1976).
 - [25] V. Sokolov and V. Zelevinsky, *Nucl. Phys.* **A504**, 562 (1989).
 - [26] T. Berggren, *Nucl. Phys.* **A109**, 265 (1968).
 - [27] A. F. J. Siegert, *Phys. Rev.* **56**, 750 (1939).
 - [28] G. Breit and E. Wigner, *Phys. Rev.* **49**, 519 (1936).
 - [29] A. Holt, T. Engeland, M. Hjorth-Jensen, and E. Osnes, *Nucl. Phys.* **A634**, 41 (1998).
 - [30] B.A. Brown and B. Wildenthal, *Ann. Rev. Nucl. Part. Sci.* **38**, 29 (1988).
 - [31] B.A. Brown, A. Etchegoyen, and W. Rae, *Tech. Rep. MSU-NSCL 524*, NSCL, Michigan State University (1994).
 - [32] A. Bohr and B. Mottelson, *Nuclear Structure*, vol I (World Scientific Publishing, 1998).
 - [33] L. Landau and E. Lifshitz, *Quantum Mechanics, Non-relativistic Theory*. Third edition (Pergamon Press, New York, 1981).
 - [34] E. Merzbacher, *Quantum Mechanics* (John Wiley and Sons, inc., New York, 1998).
 - [35] C. Davids and H. Esbensen, *Phys. Rev. C* **61**, 054302 (2000).

- [36] V. Burgov and S. Kadmsky, *Sov. J. Nucl. Phys.* **49**, 967 (1989).
- [37] V. Burgov and S. Kadmsky, *Phys. At. Nucl.* **59**, 424 (1996).
- [38] E. Wigner, *Phys. Rev.* **73**, 1002 (1948).
- [39] A. Baz, I. Zeldovich, and A. Perelomov, *Scattering, reactions and decay in nonrelativistic quantum mechanics* (Israel Program for Scientific Translations, Jerusalem, 1969).
- [40] V. Zelevinsky and A. Volya, in *Challenges of Nuclear Structure*, ed. A. Covello (World Scientific, Singapore, 2002) p. 261.
- [41] R. Dicke, *Phys. Rev.* **93**, 99 (1954).
- [42] J. Rotureau, J. Okolowicz, and M. Ploszajczak, *Phys. Rev. Lett.* **95**, 042503 (2005).
- [43] B.A. Brown, and F.C. Barker, *Phys. Rev. C* **67**, 041304 (2003).
- [44] L.V. Grigorenko and M.V. Zhukov, *Phys. Rev. C* **68** 054005 (2003).
- [45] F. C. Barker, *Phys. Rev. C* **59**, 353 (1999).
- [46] S. Cohen and D. Kurath, *Nucl. Phys.* **A73**, 1 (1965).
- [47] J. Stevenson *et al.*, *Phys. Rev. C* **37**, 2220 (1988).
- [48] J. Jänecke *et al.*, *Phys. Rev. C* **54**, 1070 (1996).
- [49] S. Nakayama *et al.*, *Phys. Rev. Lett.* **85**, 262 (2000).
- [50] *Evaluated nuclear structure data file*, <http://www.nndc.bnl.gov>.
- [51] G. V. Rogachev *et al.*, *Phys. Rev. Lett.* **92**, 232502 (2004).
- [52] A. A. Korshennikov *et al.*, *Phys. Rev. Lett.* **82**, 3581 (1999).
- [53] N. Auerbach, V. Zelevinsky, and A. Volya, *Phys. Lett. B* **590**, 45 (2004).
- [54] A. Volya and V. Zelevinsky, *J. Opt. B* **5**, S450 (2003).
- [55] T. Teichmann, *Phys. Rev.* **77**, 506 (1050).
- [56] T. Teichmann and E. Wigner, *Phys. Rev.* **87**, 123 (1952).
- [57] B.A. Brown, W. Richter, R. Julies, and B. Wildenthal, *Ann. Phys. (N.Y.)* **182**, 191 (1988).
- [58] B. Skorodumov *et al.*, submitted for publication to *Phys. Rev. C.* (2005).
- [59] V. Goldberg *et al.*, *Phys. Rev. C* **69**, 31302 (2004).
- [60] D. Tilley, C. Cheves, J. Kelley, S. Raman, H. Weller, and F. Ajzenberg-Selove, *Energy Levels of Light Nuclei, A = 3 - 20*, <http://www.tunl.duke.edu/nucldata>.
- [61] J.K. Bair, J.L.C. Ford, Jr., and C.M. Jones, *Phys. Rev.* **144**, 799 (1966).
- [62] S. F. Mughabghab, R. Kinsey, and C. Dunford, *Neutron Cross Sections Series* (Academic Press, New York, 1981).
- [63] V. McLane, C. Dunford, and P. Rose, *Neutron Cross Section Curves*, vol. 2 (Academic Press, Boston, 1988).